Original Article

A comparison of ultra-high-resolution CT target scan versus conventional CT target reconstruction in the evaluation of ground-glass-nodule-like lung adenocarcinoma

Yanyan Zhu[1#], Dailun Hou[2#], Meihong Lan[3], Xiaoli Sun[4], Xiangxing Ma[5]

[1]Division of Computed Tomography, Department of Radiology, Shandong University School of Medicine, Shandong Provincial Third Hospital, Jinan 250031, China; [2]Department of Radiology, Beijing Chest Hospital, Capital Medical University, Beijing 101149, China; [3]Department of Radiology, Shandong Chest Hospital, Jinan 250101, China; [4]Department of Computed Tomography, Beijing Shijitan Hospital, Ninth Clinical Medical College of Peking University, Capital Medical University, Beijing 100038, China; [5]Department of Radiology, Qilu Hospital, Shandong University, Jinan 250012, China

[#]These authors contributed equally to this work.

Correspondence to: Xiangxing Ma. Department of Radiology, Qilu Hospital, Shandong University, Jinan 250012, China. Email: maxiangxing123@126.com; Xiaoli Sun. Department of Computed Tomography, Beijing Shijitan Hospital, Ninth Clinical Medical College of Peking University, Capital Medical University, Beijing 100038, China. Email: sdsxl2005@126.com.

Background: The aim of this study was to determine whether the clinical value of scanned computed tomography (CT) images is higher when using ultra-high-resolution CT (U-HRCT) target scanning than conventional CT target reconstruction scanning in the evaluation of ground-glass-nodule (GGN)-like lung adenocarcinoma.

Methods: A total of 91 consecutive patients with isolated GGN-like lung adenocarcinoma were included in this study from April 2017 to June 2018. U-HRCT and conventional CT scans were conducted in all enrolled patients. Two experienced thoracic radiologists independently assessed image quality and made diagnoses. Based on the pathological results, the accuracies of U-HRCT target scanning and conventional CT target reconstruction for detecting morphological features on CT, including spiculation of GGNs, bronchial vascular bundles, solid components in the nodules, burr, vacuole, air bronchial signs, and fissure distortion, were calculated. All statistical analyses were performed using SPSS 17.0 software. Enumeration data were tested using the Chi-square test. A P value of <0.05 was considered statistically significant.

Results: When both techniques were compared with the pathological findings, the detection rate for CT images obtained using U-HRCT target scanning and conventional CT target reconstruction with regard to the spiculation of GGNs, bronchial vascular bundles, and solid components in the nodules were 78% *vs.* 61.5%, 72.5% *vs.* 54.9%, 65.9% *vs.* 49.5%, respectively. The presence of the spiculation of GGNs, bronchial vascular bundles, and solid components in the nodules in U-HRCT target scanning was significantly higher than that in conventional CT target reconstruction (all P<0.05). However, no significant difference was observed between the two techniques with regard to the burr, vacuole, air bronchial signs, and fissure distortion (all P>0.05).

Conclusions: When viewing GGNs, the detection rate was higher for U-HRCT target scanning than for conventional CT target reconstruction, and this improvement significantly enhanced the diagnostic accuracy of early lung adenocarcinoma.

Keywords: Ultra-high-resolution CT target scan (U-HRCT target scan); conventional CT target reconstruction; ground-glass opacity; lung adenocarcinoma

Submitted Dec 17, 2018. Accepted for publication Jun 11, 2019.
doi: 10.21037/qims.2019.06.09
View this article at: http://dx.doi.org/10.21037/qims.2019.06.09

Introduction

Lung adenocarcinoma can be classified as atypical adenomatous hyperplasia (AAH), adenocarcinoma *in situ* (AIS), micro-invasive (MIA), and invasive adenocarcinoma (IAC). AAH and AIS are considered pre-invasive (PI) lesions. It is important to differentiate among PI, MIA, and IAC lesions (1). High-resolution computed tomography (HRCT) can been applied in the lungs, and HRCT images have greatly improved the display of the fine structures of lung tissues, such as surrounding pulmonary vessels, peripheral bronchioles, and lobular septa (2). HRCT can also improve image quality and provide clearer images of ground-glass nodules (GGNs) (3-6). Lung adenocarcinoma can appear as GGNs on chest HRCT (7-11). Sakurai *et al.* suggested that the early and accurate diagnosis of GGN malignancy significantly improved the treatment and prognosis of patients (12). However, the spatial resolution of traditional HRCT scans ranges from 0.23 to 0.35 mm (13), and Kakinuma *et al.* (14) showed that U-HRCT can detect cracks with a diameter of 0.12 mm. U-HRCT provides a clearer image of the relationship between nodules and bronchioles than HRCT, especially when reconstructing bronchial features. According to the latest Fleischner Society recommendations (15), it takes 3.6 years for a solid component to appear in a subsolid nodule. Thus, it is important to improve the CT scanning technique and the diagnostic accuracy of GGN-like lung adenocarcinoma.

However, to our knowledge, no prospective clinical study has compared the image quality or diagnostic accuracy of U-HRCT and conventional CT target construction for the detection of GGN-like lung adenocarcinoma. Hence, the aims of this study were to compare the image quality between U-HRCT target scans and conventional CT target reconstruction in GGN-like lung adenocarcinoma and investigate the effect of U-HRCT target scans in the diagnosis of early lung adenocarcinoma.

Methods

Patients

This prospective clinical study was approved by the ethical committee of our institutional review board, and written informed consent was obtained from all the patients. A total of 91 consecutive patients with isolated GGN-like lung adenocarcinoma were included in this study from April 2017 to June 2018. The inclusion criteria were as follows: (I) isolated GGN of the lung with a diameter of 8 mm to 3 cm that was pathologically confirmed as AAH, AIS, MIA, or IAC; (II) no mixed lesions, such as strips, exudation, emphysema, cysts, or miliary nodules, around the lesions; (III) both U-HRCT target scanning and conventional CT target construction performed for all enrolled patients. After CT examination, all 91 GGNs underwent surgical resection and were confirmed by pathology. They were classified into three groups: a PI group (n=30) that included 9 cases of AAH and 21 cases of AIS, an MIA group (n=25), and an IAC group (n=36).

Protocol for U-HRCT target scan and conventional CT target construction

A 128-row CT scanner (Brilliance iCT, Philips, Best, The Netherlands) was applied in this study. Two sets of images (U-HRCT target scans and conventional CT target construction) were obtained in each patient using the same CT scanner. The patients were trained in breathing depth and frequency before scanning. They were placed in the supine position and examined while they held their breath at the end of a deep inhalation. Intravenous contrast material was not used. The scanning range of conventional CT target construction was from the tip of the lung to the base of the lung. The parameters used for conventional CT scanning were as follows: collimation 0.625 mm ×128; pitch, 1.08:1; 120 kV; 250 mA; scan time, 5–7 s; field of view (FOV), 400 mm; reconstruction layer thickness and spacing, 5 mm; image matrix, 512×512. After a GGN was discovered, conventional CT target reconstruction was performed on the lesion. The thicknesses and intervals of the reconstructed layers were 1 mm.

When a GGN was found on conventional CT scans, a U-HRCT target scan was performed on the same ground-glass nodular after agreement was obtained from the patient and a family member. The median interval between the U-HRCT target scan and the conventional CT scan was 0 days. The scanning range of a U-HRCT target scan was 1 cm above and below the GGN. The parameters used for the U-HRCT target scan were as follows: collimation, 0.625 mm ×128; pitch, 0.64:1; 120 kV; 300 mA; scanning time, 1 to 3 s; FOV, 140 mm; reconstruction layer thickness and spacing, 0.67 mm; and image matrix, 1,024×1,024.

CT image analysis

All CT images were reconstructed in Philips Extended Brilliance Workspace v4.5 (Philips Medical Systems). The

lung window settings for both conventional CT target construction and U-HRCT target scans were a width of 1,450 HU and a center of –520 HU. The U-HRCT target scan and conventional CT target construction images were displayed side by side in a random manner, and any annotations related to the scanned information were deleted. The images were independently assessed by two experienced radiologists with 10 and 15 years of experience in thoracic imaging diagnosis. The two experienced radiologists independently read the films without knowing the pathological results. Any disagreements over the conclusions were resolved by consensus. A "Yes" or "None" was recorded for the seven CT morphological features of the two CT examination techniques. If the result was difficult to judge, "None" was selected. The following seven CT morphological features were selected for statistical analysis: the spiculation of GGNs, bronchial vascular bundles, solid components in the nodules, burr sign, vacuoles sign, air bronchial sign, and fissure distortion. Based on the pathological results, the accuracies (detection rates) of U-HRCT target scanning and conventional CT target reconstruction for the above morphological features were calculated and compared.

Pathological assessment

Pathological results were reviewed from pathologic reports. Pathologic subtypes were evaluated according to the new pathologic classification (8). AAH and AIS were defined as tumours ≤0.5 and ≤3 cm, respectively, with a pure lepidic pattern. MIA was defined as a tumour ≤3 cm with a lepidic predominant pattern and ≤5 mm of stromal invasion. IAC was classified according to the predominant pattern, mainly including lepidic, acinar, papillary, micropapillary, or solid adenocarcinoma. Of note, a lepidic pattern of IAC was defined as a tumour ≥3 cm with a predominant lepidic pattern and ≥5 mm of stromal invasion.

For each case, CT images obtained using U-HRCT target scanning and a conventional CT target reconstruction were compared to the pathological findings. Pathologically, GGNs can represent AAH, AIS, MIA and IAC. On CT, AAH appears as a well-defined round or oval pure GGN. AIS and MIA show neither lymphatic metastasis nor vascular or fissure distortion. Most IAC lesions present as sub-solid nodules. As lesion infiltration increases, the probability of detecting morphological features on CT such as the spiculation of GGNs, solid components inside the nodules, bronchial vascular bundles, and air bronchial sign increases.

It has been shown that CT features of GGNs correlate well with the pathological classification of adenocarcinoma (4). On pathological examination, GGNs show focal interstitial thickening with collagen fiber deposition, type 2 pneumocyte proliferation, and macrophage collection in the airspace. The presence of spiculation of nodules and bronchial vascular bundle on GGNs tended to indicate malignancy, likely because with the increase in the degree of invasion, the tumor cell arrangement on alveolar walls became dense and thickened, thus presenting a clearer tumor-lung interface on CT imaging. The solid component in GGNs corresponded to areas of structural collapse of alveoli or fibroblastic proliferation. The mechanism of vacuole sign, air bronchial sign, fissure distortion possibly is adjacent to traction of the fibrous components within the lesion on the surrounding normal tissue (14).

Statistical analysis

Statistical analyses of the data were performed using the SPSS 17.0 software package (SPSS Inc., Chicago, IL, USA). Seven CT morphological features (spiculation of GGNs, bronchial vascular bundles, solid components in the nodules, burr sign, vacuoles sign, air bronchial sign, and fissure distortion) and the accuracies (detection rates) of U-HRCT target scan and conventional CT target construction were determined using Chi-square tests. A P value of <0.05 was considered statistically significant.

Results

In all, 91 patients (42 males and 49 females) with a total of 91 GGNs were included the final analysis. The mean age was 55±8 years (range, 38–73 years old). All patients underwent CT examination using a U-HRCT target scan and conventional CT target construction. The mean radiation dose used in the U-HRCT target scans was 175.4±42.8 mGy·cm (range, 103.5–299.8 mGy·cm).

Of the 91 cases, 30 were diagnosed by pathology as pre-invasive lesions (AAH, AIS) (n=30), 25 as MIA (n=25), and 36 as IAC (n=36). According to U-HRCT target scan-based diagnosis, 28 were pre-invasive lesions (AAH, AIS) (n=28), 28 were MIA (n=28), and 35 were IAC (n=35); meanwhile, conventional CT target reconstruction resulted in the diagnosis of 37 pre-invasive lesions (n=37), 24 MIA lesions (n=24), and 30 IAC lesions (n=30). In all, there was agreement between U-HRCT target scan and pathology results in 86 cases (n=86, 94.5%) and between conventional CT target reconstruction and pathology results in 75 cases

Table 1 Comparison of U-HRCT target scan and conventional CT target reconstruction in diagnosis of seven CT morphological features of ground-glass lung adenocarcinoma (total number =91)

	U-HRCT target scan, n (%)	Conventional CT target construction, n (%)	χ^2	P value
Seven CT morphological features				
Spiculation of nodule	71 (78.0)	56 (61.5)	5.863	0.015
Bronchial vascular bundle	66 (72.5)	50 (54.9)	6.086	0.014
Solid component in ground-glass nodules	60 (65.9)	45 (49.5)	5.065	0.024
Burr sign	34 (37.4)	29 (31.9)	0.319	0.572
Vacuole sign	22 (24.2)	18 (19.8)	0.513	0.474
Air bronchial sign	28 (30.8)	26 (28.6)	0.105	0.746
Fissure distortion	30 (33.0)	21 (23.1)	2.207	0.137
Consistent with pathology results	86 (94.5)	75 (82.4)	6.513	0.011

U-HRCT, ultra-high-resolution computed tomography.

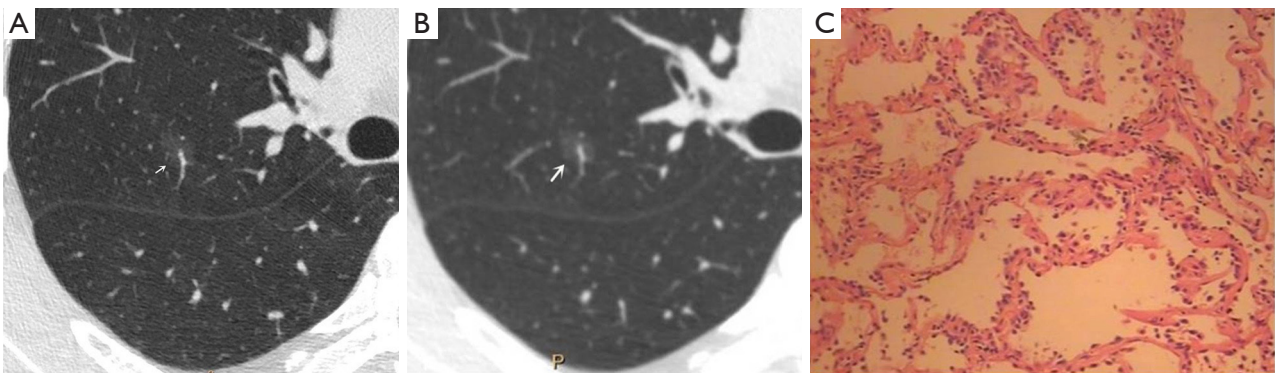

Figure 1 Male, 53 years old. A U-HRCT target scan image shows clear speculation and a bronchial vascular bundle in the ground-glass nodule (A). A conventional CT target reconstruction image shows unclear spiculation and bronchial vascular bundles in the ground-glass nodule (B). The pathological image depicts the tumour cells being sparsely arranged along the alveolar wall, thus presenting a ground-glass nodule and a clearer tumour-lung interface on CT imaging. The pathological results confirmed the presence of atypical adenomatous hyperplasia (C, HE staining, 200×). U-HRCT, ultra-high-resolution computed tomography. The arrows point out the lesions.

(n=75, 82.4%). In this study, when the results of both techniques were compared with pathological findings, the diagnostic accuracy of U-HRCT was significantly higher than that of conventional CT target reconstruction (χ^2 =6.513, P=0.011).

The results of the comparison of U-HRCT target scanning and conventional CT target reconstruction for the diagnosis of seven CT morphological features of GGN-like lung adenocarcinoma are shown in *Table 1*. The difference in accuracy between U-HRCT target scanning and conventional CT target reconstruction was statistically significant with regard to the spiculation of nodules, bronchial vascular bundles, and solid components in pulmonary GGNs (all P<0.05). However, the difference of accuracy between U-HRCT target scanning and conventional CT target reconstructions was not statistically significant with regard to the identification of the burr sign, vacuole sign, air bronchial sign, and fissure distortion (all P>0.05).

CT images of U-HRCT target scanning and conventional CT target reconstruction obtained at different pathological stages of lung adenocarcinoma are shown in *Figures 1-5*. In this study, the PI lesions were slightly dense with homogeneous density, and normal lung tissue could be implicitly seen. The boundary of the lesion was clear, and the

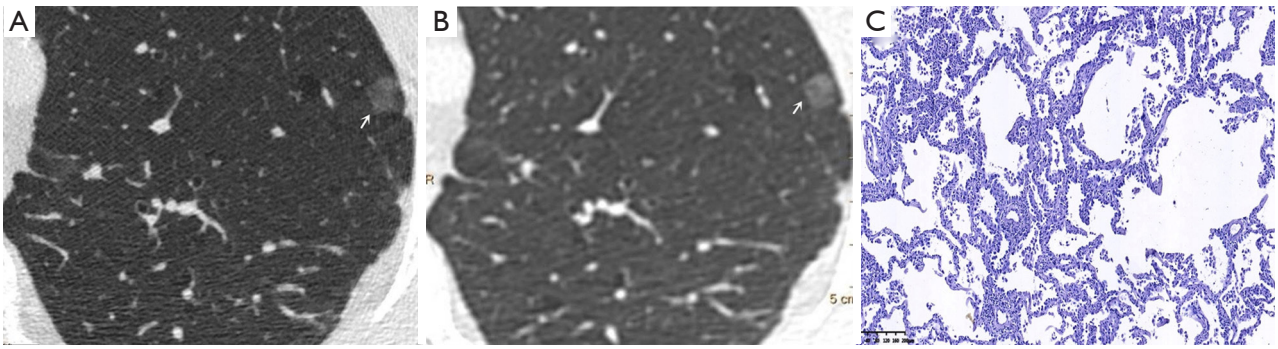

Figure 2 Male, 65 years old. A U-HRCT target scan image (A) and a conventional CT target reconstruction image (B) show clear and sharp spiculation of the ground-glass nodule. The pathological image indicates that the tumour cells are tightly arranged along the alveolar wall, thus presenting a ground-glass nodule and a clearer tumour-lung interface on CT imaging. The pathological results confirmed the presence of adenocarcinoma *in situ* (C, HE staining, 100×). U-HRCT, ultra-high-resolution computed tomography. The arrows point out the lesions.

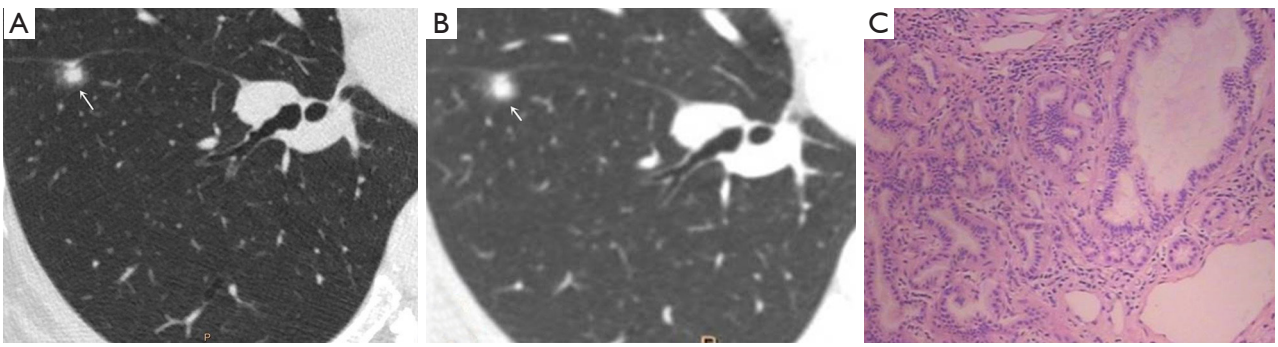

Figure 3 Female, 48 years old. U-HRCT target scan (A) shows the clear spiculation of the ground-glass nodule. The central solid component in the nodule is clearly separated from the surrounding ground-glass opacity, and the adjacent fissure is distorted and thickened. A conventional CT target reconstruction (B) shows that the central solid component in the nodule is unclearly separated from the surrounding ground-glass opacity, while the spiculation of the ground-glass nodule is blurred. The adjacent fissure is distorted, and the thickness is not obvious. The pathological image indicates tumour infiltration into the matrix leading to the contraction of the elastic tissues of the lung with the adjacent fissure distortion, thus presenting a central solid component in the nodule on CT imaging. The pathological results confirmed the presence of microinvasive adenocarcinoma (C, HE staining, 100×). U-HRCT, ultra-high-resolution computed tomography. The arrows point out the lesions.

shape of the lesion was spherical (*Figures 1,2*). With increases in lesion infiltration, the bronchial vascular bundles of MIA and IAC thickened, accompanied by the appearance of solid components in GGNs, vacuole sign, air bronchial sign, burr sign, and fissure distortion (*Figures 3-5*).

Discussion

Pulmonary GGNs reflect an increase in the density of local lung tissues that is insufficient to mask the passage of the bronchial vessels (6). The long-term view of lung adenocarcinoma organization is that the cancer cells grow along the alveolar wall and gradually infiltrate into the surrounding tissues. Therefore, most pre-invasive lesions (AAH, AIS) present as pulmonary GGNs (*Figures 1,2*). As the pathological grade progresses, the volume and density of the lesions gradually increases (13,16). In this study, the boundaries of MIA and IAC nodules were mostly blurred, their internal solid components increased, and some bronchial vascular bundles became thicker (*Figures 3-5*). According to reports published by Sakurai *et al.* (12) and Terasaki *et al.* (17), AIS and MIA should show no lymphatic metastasis and no vascular or fissure distortion. Most IAC lesions present as sub-solid

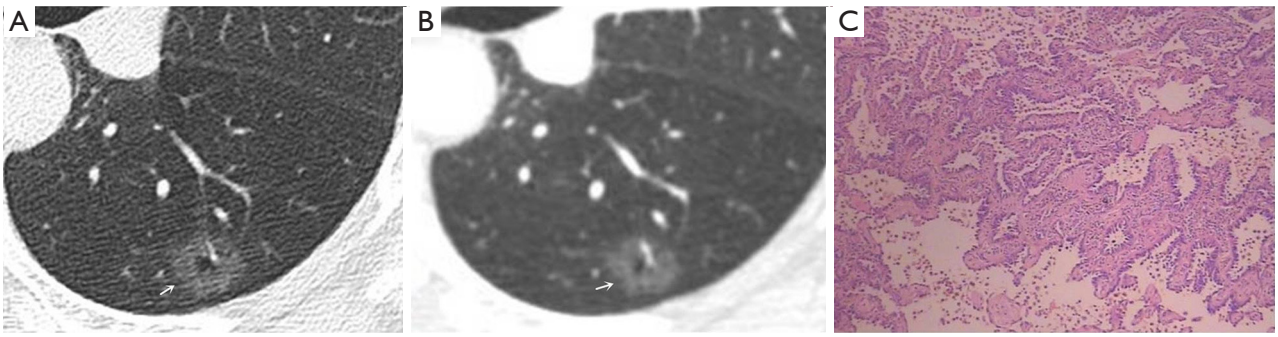

Figure 4 Female, 57 years old. A U-HRCT target scan (A) shows a vacuole sign in the GGN. A conventional CT target reconstruction (B) shows that the vacuole sign in the nodule is unclearly separated from the surrounding ground-glass opacity. The pathological image indicates tumour infiltration into the matrix leading to the contraction of the elastic tissues of the lung, thus presenting a vacuole sign (normal lung tissue inside the nodule) on CT imaging. The pathological results confirmed the presence of invasive adenocarcinoma (C, HE staining, 200×). U-HRCT, ultra-high-resolution computed tomography; GGN, ground-glass nodule. The arrows point out the lesions.

Figure 5 Female, 49 years old. A U-HRCT target scan (A) clearly shows the bronchial vascular bundle inside the nodule and burr sign at the nodule edge. A conventional CT target reconstruction (B) shows the uneven density of the nodule, but the bronchial vascular bundle and burr sign are unclear. The pathological image indicates tumour infiltration into the matrix leading to the contraction of the elastic tissues of the lung, with the contracted fibres pulling the surrounding normal lung tissue and the bronchial vascular bundle, thus presenting a burr sign and a bronchial vascular bundle on CT imaging. The pathological results confirmed the presence of invasive adenocarcinoma (C, HE staining, 200×). U-HRCT, ultra-high-resolution computed tomography. The arrows point out the lesions.

nodules. Saito *et al.* (18) reported that as lesion infiltration increases, the probability of air bronchial sign increases, probably because tumour infiltration into the matrix leads to the contraction of the elastic tissues of the lung, with the contracted fibers pulling on the surrounding normal lung tissue. Clear indication of CT morphological features such as the spiculation of GGNs, solid components inside the nodules, bronchial vascular bundles, and air bronchial sign, support the pathological staging of lung adenocarcinoma. The results of this study show that the quality of the imaging of morphological features was better for U-HRCT target scans than for conventional CT target reconstruction with regards to the spiculation of GGNs and the presence of solid components inside the nodules and bronchial vascular bundles.

The HRCT morphological features of pulmonary GGNs have been correlated with pathological staging (19,20). The analysis of HRCT morphological features is helpful for the differential diagnosis and pathological staging of lung adenocarcinoma. The tumor cells observed in AAH and AIS are sparsely arranged along the alveolar wall, and their growth range is also loose (13). Normal alveolar structures should be present in the diseased tissue (*Figures 1C*,*2C*), and these were more clearly shown on U-HRCT target scans than by conventional CT target reconstruction (*Figures 1A*,*B*,*2A*,*B*). The tumour-lung interface was more

blurred on conventional CT target reconstruction; however, U-HRCT target scans clearly showed the nodule margins (*Figures 3A,B,4A,B,5A,B*), facilitating the pathological staging of GGNs.

In this study, the conventional CT target reconstruction procedure was based on conventional CT scans with a thickness of 1 mm and a 512×512 matrix. The U-HRCT target scans were performed at a thickness of 0.67 mm with a 1,024×1,024 matrix. The matrix size was related to the quality of the reconstructed image. Given sampling fields of the size, a larger matrix will contain more pixels and therefore have a higher resolution and better image quality after reconstruction. Spatial resolution, also called high-contrast resolution, refers to the ability of a CT-scanned image to resolve two tiny structures that are very close together and describes the ability of a technique to resolve two adjacent points on a fault and is mainly based on the size of the detector's collimation aperture. The use of thinner layers during the scan provides a greater number of images and a better recombination effect. In theory, U-HRCT target scans provide a higher resolution and better image quality than can be achieved by conventional CT target constructions, and the results of this study support this notion. According to the recommendations of the Fleischner Society for lung cancer screening, if a lesion has been identified in 5-mm slices obtained on a chest CT, a follow-up procedure should be performed using 1- or 1.5-mm slices. Thus, in our study, we chose 1 mm as the image layer thickness for conventional CT scan target reconstruction.

In this study, the difference between U-HRCT target scans and conventional CT target reconstruction was statistically significant with regard to the spiculation of nodules and the presence of bronchial vascular bundles and solid components in pulmonary GGNs, with the former being clearer than the latter. However, the difference between U-HRCT target scans and conventional CT target reconstructions was not statistically significant with regard to the identification of burr sign, vacuole sign, air bronchial sign, and fissure distortion. Sheshadri *et al.* (21) reported that obtaining U-HRCT target scans using a small FOV significantly improved the spatial resolution of images. Our results show that U-HRCT target scans provided better image quality in mixed component ground-glass lung adenocarcinoma (*Figure 5*).

This study has three limitations. First, U-HRCT target scans are more susceptible to heartbeat and respiratory movements and more easily produce image artifacts. Thus, when using U-HRCT-scanned images, small pulmonary nodules close to the heart were not clear. Second, U-HRCT target scans need to be performed twice, unlike a conventional CT scan, and this increases the patient's radiation dose. Third, the number of patients in this study was small. With regard to the 7 morphological features obtained during CT in GGN-like lung adenocarcinoma, only three features (the spiculation of nodules and the presence of bronchial vascular bundles and solid components in GGNs) were significantly different between CT target reconstruction and U-HRCT. Therefore, the diagnostic value of U-HRCT target scans for early lung adenocarcinoma needs to be further studied.

In summary, concerning the CT morphological features of ground-glass lung adenocarcinoma, which include the spiculation of nodules and the presence of bronchial vascular bundles and solid components inside the nodules, a U-HRCT target scan will produce better image quality than that achieved by conventional CT target reconstructions. These findings suggest that U-HRCT target scanning provides better image quality than CT target reconstruction when viewing GGNs and therefore significantly contributes to improving diagnostic accuracy in early lung adenocarcinoma.

Acknowledgments

None.

Footnote

Conflicts of Interest: The authors have no conflicts of interest to declare.

Ethical Statement: The study was conducted in accordance with the Committee for Human Research at our institution and followed all regulations. Informed consent was obtained before scans.

References

1. Travis WD, Brambilla E, Riely GJ. New pathologic classification of lung cancer: relevance for clinical practice and clinical trials. J Clin Oncol 2013;31:992-1001.
2. Todo G, Ito H, Nakano Y, Dodo Y, Maeda H, Murata K, Odori T, Torizuka K, Izumi T, Oshima S. High resolution CT (HR-CT) for the evaluation of pulmonary peripheral disorders. Rinsho Hoshasen 1982;27:1319-26.
3. Carter D, Vazquez M, Flieder DB, Brambilla E, Gazdar A, Noguchi M, Travis WD, Kramer A, Yip R, Yankelevitz DF, Henschke CI. Comparison of pathologic findings

of baseline and annual repeat cancers diagnosed on CT screening. Lung Cancer 2007;56:193-9.
4. Goo JM, Park CM, Lee HJ. Ground-glass nodules on chest CT as imaging biomarkers in the management of lung adenocarcinoma. AJR Am J Roentgenol 2011;196:533-43.
5. Henschke CI, Yankelevitz DF, Mirtcheva R, McGuinness G, McCauley D, Miettinen OS. CT screening for lung cancer: frequency and significance of part-solid and nonsolid nodules. AJR Am J Roentgenol 2002;178:1053-7.
6. Park CM, Goo JM, Lee HJ, Lee CH, Chun EJ, Im JG. Nodular ground-glass opacity at thin-section CT: histologic correlation and evaluation of change at follow-up. Radiographics 2007;27:391-408.
7. Jang HJ, Lee KS, Kwon OJ, Rhee CH, Shim YM, Han J. Bronchioloalveolar carcinoma: focal area of ground-glass attenuation at thin-section CT as an early sign. Radiology 1996;199:485-8.
8. Meng Y, Liu CL, Cai Q, Shen YY, Chen SQ. Contrast analysis of the relationship between the HRCT sign and new pathologic classification in small ground glass nodule-like lung adenocarcinoma. Radiol Med 2019;124:8-13.
9. Seemann MD, Staebler A, Beinert T, Dienemann H, Obst B, Matzko M, Pistitsch C, Reiser MF. Usefulness of morphological characteristics for the differentiation of benign from malignant solitary pulmonary lesions using HRCT. Eur Radiol 1999;9:409-17.
10. Yasaka K, Katsura M, Hanaoka S, Sato J, Ohtomo K. High-resolution CT with new model-based iterative reconstruction with resolution preference algorithm in evaluations of lung nodules: Comparison with conventional model-based iterative reconstruction and adaptive statistical iterative reconstruction. Eur J Radiol 2016;85:599-606.
11. Zwirewich CV, Vedal S, Miller RR, Muller NL. Solitary pulmonary nodule: high-resolution CT and radiologic-pathologic correlation. Radiology 1991;179:469-76.
12. Sakurai H, Maeshima A, Watanabe S, Suzuki K, Tsuchiya R, Maeshima AM, Matsuno Y, Asamura H. Grade of stromal invasion in small adenocarcinoma of the lung: histopathological minimal invasion and prognosis. Am J Surg Pathol 2004;28:198-206.
13. Tsukagoshi S, Ota T, Fujii M, Kazama M, Okumura M, Johkoh T. Improvement of spatial resolution in the longitudinal direction for isotropic imaging in helical CT. Phys Med Biol 2007;52:791-801.
14. Kakinuma R, Moriyama N, Muramatsu Y, Gomi S, Suzuki M, Nagasawa H, Kusumoto M, Aso T, Muramatsu Y, Tsuchida T, Tsuta K, Maeshima AM, Tochigi N, Watanabe S, Sugihara N, Tsukagoshi S, Saito Y, Kazama M, Ashizawa K, Awai K, Honda O, Ishikawa H, Koizumi N, Komoto D, Moriya H, Oda S, Oshiro Y, Yanagawa M, Tomiyama N, Asamura H. Ultra-High-Resolution Computed Tomography of the Lung: Image Quality of a Prototype Scanner. PLoS One 2015;10:e0137165.
15. MacMahon H, Naidich DP, Goo JM, Lee KS, Leung ANC, Mayo JR, Mehta AC, Ohno Y, Powell CA, Prokop M, Rubin GD, Schaefer-Prokop CM, Travis WD, Van Schil PE, Bankier AA. Guidelines for Management of Incidental Pulmonary Nodules Detected on CT Images: From the Fleischner Society 2017. Radiology 2017;284:228-43.
16. Borczuk AC. Assessment of invasion in lung adenocarcinoma classification, including adenocarcinoma in situ and minimally invasive adenocarcinoma. Mod Pathol 2012;25 Suppl 1:S1-10.
17. Terasaki H, Niki T, Matsuno Y, Yamada T, Maeshima A, Asamura H, Hayabuchi N, Hirohashi S. Lung adenocarcinoma with mixed bronchioloalveolar and invasive components: clinicopathological features, subclassification by extent of invasive foci, and immunohistochemical characterization. Am J Surg Pathol 2003;27:937-51.
18. Saito H, Yamada K, Hamanaka N, Oshita F, Ito H, Nakayama H, Yokose T, Kameda Y, Noda K. Initial findings and progression of lung adenocarcinoma on serial computed tomography scans. J Comput Assist Tomogr 2009;33:42-8.
19. Lee SM, Park CM, Goo JM, Lee HJ, Wi JY, Kang CH. Invasive pulmonary adenocarcinomas versus preinvasive lesions appearing as ground-glass nodules: differentiation by using CT features. Radiology 2013;268:265-73.
20. Zhang L, Yankelevitz DF, Carter D, Henschke CI, Yip R, Reeves AP. Internal growth of nonsolid lung nodules: radiologic-pathologic correlation. Radiology 2012;263:279-86.
21. Sheshadri A, Rodriguez A, Chen R, Kozlowski J, Burgdorf D, Koch T, Tarsi J, Schutz R, Wilson B, Schechtman K, Leader JK, Hoffman EA, Castro M, Fain SB, Gierada DS. Effect of Reducing Field of View on Multidetector Quantitative Computed Tomography Parameters of Airway Wall Thickness in Asthma. J Comput Assist Tomogr 2015;39:584-90.

Cite this article as: Zhu Y, Hou D, Lan M, Sun X, Ma X. A comparison of ultra-high-resolution CT target scan versus conventional CT target reconstruction in the evaluation of ground-glass-nodule-like lung adenocarcinoma. Quant Imaging Med Surg 2019;9(6):1087-1094. doi: 10.21037/qims.2019.06.09

